Surface Science 631 (2015) 258–266

Contents lists available at ScienceDirect

Surface Science

journal homepage: www.elsevier.com/locate/susc

RhPt/graphite catalysts for CO electrooxidation: Performance of mixed metal and alloyed surfaces

L. Fang [1], F.J. Vidal-Iglesias [2], S.E. Huxter, G.A. Attard *, P.B. Wells

School of Chemistry, Main Building, Cardiff University, Cardiff CF10 3AT, UK

ARTICLE INFO

Available online 5 July 2014

Keywords:
PtRh surface alloy
Forced deposition
CO electro-catalytic oxidation
Cyclic voltammetry
X-ray photoelectron spectroscopy

ABSTRACT

Cyclic voltammetry (CV) and X-ray photoelectron spectroscopy (XPS) have been used to characterise novel PtRh mixed metal and surface alloyed active phases supported on 5% Pt/graphite catalysts (5% Pt/G). The active phases could be prepared using forced deposition or a combination of forced deposition and thermal annealing in a flowing 5% hydrogen in argon gas mixture at 700 K. The protocols employed originate directly from previous single crystal studies of Rh on Pt{100} whereby Rh overlayers (either singly adsorbed or as a 'sandwich structure' of alternate Pt/Rh/Pt layers) could be transformed into surface PtRh alloys by careful thermal annealing. We demonstrate that this method is also successful for the preparation of active supported catalysts for CO electrooxidation whereby a peak potential as low as 0.60 V (Pd/H) for the CO oxidation is reported (0.12 V lower than that on 5% Pt/G). Moreover, the onset potential for CO stripping is lowered to 0.33 V (Pd/H). The presence of alloyed PtRh phases gives rise to a small but reproducible 0.1–0.2 eV shift to higher binding energy of the Pt $4f_{7/2}$ XPS peak together with strongly modified Pt and Rh electrosorption features in the CV which correlate with changes in surface composition. Unusual kinetic behaviour in the CO stripping peaks from the PtRh catalyst as a function of CO coverage is ascribed to competition between electrochemical oxide on Rh and CO-induced blocking of electrochemical oxide formation sites at the highest CO coverage. For PtRh alloys, the onset of electrochemical oxide formation shifts to more positive potentials relative to Rh overlayers and so a different behaviour towards CO electrooxidation is observed.

1. Introduction

Twenty years ago, we submitted two papers to the IUVSTA conference in San Benedetto del Tronto concerning the electrochemical and UHV characterisation of metal deposition on single crystal electrodes [1,2]. One of these systems was Rh on Pt{111} whereby strong deviations from Frank-van der Merwe growth were observed together with surface alloying at elevated temperatures [2]. More importantly at that time however, correlations between the potentials at which various electrosorption states occurred and first/second layer/bulk Rh (as measured using Auger electron spectroscopy) were noted. This meant that certainly, for Rh in a monolayer directly bonded to the Pt{111} surface, a specific electrochemical response could be measured that was proportional to surface coverage. Since then, many groups have used the variation in single crystal CV peak positions and intensity to characterise both clean and surface-modified nanoparticles and supported catalysts in exquisite detail [3–10]. In the present study, we utilise such measurements to characterise a series of mixed metal and alloyed PtRh supported catalysts and investigate their behaviour towards CO electrooxidation for potential fuel cell applications. (See Table 1.)

The challenge of ever decreasing fossil fuel supplies together with ongoing global climate change has initiated a resurgence of interest in the use of fuel cells for efficient and clean sources of electrical power. By far the most important materials presently used include PtRu alloys for the anodic reaction (hydrogen oxidation) and Pt alloys for the cathodic reaction (oxygen reduction) since bimetallic catalysts exhibit good activity and CO tolerance in relation to low-temperature fuel cells [7,11–29]. PtRu electrodes have been used as commercial catalysts for hydrogen oxidation in fuel cells for some time now because of their high intrinsic electrocatalytic activity during hydrogen oxidation and marked tolerance towards CO poisoning [14–19]. Nevertheless, leaching of Ru under operating conditions together with ambiguity concerning the actual "location" of the Ru within Pt nanoparticles of the electrocatalyst is still a controversial issues for the anodic reaction. Hence, a considerable research effort has been expended on another promising bimetallic system, namely PtRh [2,30–35]. More recently, a novel approach for the synthesis of PtRh{100} surface alloys supported

* Corresponding author. Tel.: +44 29 20874023; fax: +44 29 20874030.
E-mail address: attard@cardiff.ac.uk (G.A. Attard).
[1] Permanent address: School of Chemistry and Chemical Engineering, Shanxi University, Taiyuan 030006, PR China.
[2] Permanent address: Instituto Universitario de Electroquímica, Universidad de Alicante, Apartado 99, 03080 Alicante, Spain.

http://dx.doi.org/10.1016/j.susc.2014.06.026

on Pt{100} single crystal based on controlled thermal annealing of PtRhPt and Rh adlayers has been reported by ourselves [5]. In this work, it was found that flame annealing in the presence of oxygen is crucial in order to generate Rh-rich PtRh{100} alloys. So-called PtRhPt sandwich structures were concluded to be the best strategy to form well-defined PtRh surface alloys. The CO stripping potential on PtRh alloys on Pt{100} was 170 mV lower than on a pure Pt{100} surface, which was quite similar to the value reported for PtRu alloys [12,14,19] indicating that certain PtRh{100} alloys may be considered as promising electrocatalyst in CO tolerant hydrogen fuel cells.

Pt–Rh nanoparticles for anode catalysts in fuel cells have been reported recently [36–38]. Lima et al. studied carbon-dispersed Pt–Rh (1:1) nanoparticles for ethanol electrooxidation and it was found that the electrochemical stripping of CO and the electrochemical ethanol oxidation were slightly faster on the Pt–Rh electrocatalysts compared to Pt/C [37]. Using FTIR and DEMS measurement, they ascribed C–C bond breaking by Rh to the higher activity of PtRh electrocatalysts in ethanol oxidation. Gupta and Datta demonstrated a comparative study concerning the catalytic activity for ethanol oxidation of electrodeposited Pt and Pt–Rh alloys on graphite plates [36]. They found that PtRh alloys with atomic composition $Pt_{74}Rh_{26}$ showed the best behaviour towards ethanol oxidation, and they also ascribed the enhancement in electrocatalytic activity to an improvement in C–C bond dissociation rather than to a bifunctional mechanism. More recently, Kowal et al. synthesised carbon supported Pt, PtRh, Pt–SnO_2 and Pt–Rh–SnO_2 nanoclusters using the polyol method and characterised the catalysts by TEM, XRD and cyclic voltammetry [38]. In this work, they found that Pt and Rh were deposited directly on SnO_2 in the ternary catalyst Pt–Rh–SnO_2 which showed better activity than either PtRh/C or Pt/C due to a tri-functional mechanism, i.e. Pt for adsorption of the ethanol molecule, Rh for facilitating C–C bond dissociation and SnO_2 for the oxidative removal of CO_{ads} produced from C–C bond splitting.

In the present study, we endeavour to take protocols for producing well-defined PtRh alloys and bimetallic surfaces on single crystal electrodes and apply these to facilitate synthesis of high surface area catalysts thus bridging the materials gap between single crystal studies and 'real' supported catalysts. A combination of CV and XPS allows for detailed analysis of the surface of the catalysts and highlights the crucial role of electrochemical oxide phases during the electrooxidation of CO.

2. Experimental

5% Pt/graphite powder (Johnson Matthey, Assay 4.92%, labelled as 5% Pt/G) was heated in 5% H_2/Ar at 700 K for 4 h before use. This catalyst had been fully characterised previously using BET and TEM after this treatment [39] and gave rise to a Pt metal surface area of 1 m^2/g together with an average particle size of 9 ± 3 nm. The Pt nanoparticles were strongly facetted after this treatment forming predominantly hexagonal structures. The deposition of rhodium was carried out using $RhCl_3$ solution (0.01 M) which was prepared by dissolving $RhCl_3$ powder (Johnson Matthey, Assay 42.4%) in ultra-pure water (Millipore-MilliQ, resistivity not less than 18.2 MΩ·cm). Rh_x/Pt/G samples (x = number of monolayer equivalents — see later) were prepared by adding a fixed amount of 5% Pt/G powder (approximately 0.3–0.4 g) into a hydrogen bubbler but with different volumes of rhodium solution and bubbling for 40 min to ensure that all Rh was reduced and deposited. This process of adsorbing metal is called the 'forced deposition' method [20,40–42]. After drying in an oven at 350 K, the catalysts are referred to at this stage as 'fresh'. The following equation was used to generate a 'monolayer equivalent' of Rh deposited on Pt given the molarity and volume V of Rh solution added together with a Pt surface area of 1 m^2/g of catalyst and assuming all Rh ions are reduced (see Table 1):

$$\text{Area of Rh atoms}: 0.0094 \times \mathbf{V} \times 10^{-3} \times 6.02 \times 10^{23} \times 3.1416 \times \left(1.34 \times 10^{-10}\right)^2 = (0.3192\mathbf{V})\,m^2.$$

All the surface alloys were prepared using our recently developed "sandwich structure annealing" methodology [5–7]. Both Rh and $Pt_xRh_yPt_z$ sandwich-like deposits were prepared by means of the so-called forced deposition method referenced above, where x, y and z are the amounts of Pt and Rh in each of the sandwich layers in terms of monolayer equivalents [5]. Chloroplatinic acid (Johnson Matthey, Assay 46.6%) was used for Pt deposition (2 mM). A similar method to that for Rh was used to calculate the monolayer equivalents of Pt in the layer. Using the same method, Pt, Rh and Pt adlayers were deposited in turn to prepare $Pt_xRh_yPt_z$/5% Pt/G samples as well. The catalyst particle suspensions were then washed with ultra-pure water several times and vacuum filtered in order to remove all traces of chloride ions. Chlorine atoms could not be detected in subsequent XPS analysis of the washed catalysts. All the obtained 'fresh' sandwich layer catalysts were then dried at room temperature and subsequently in 5% H_2/Ar at 700 K for 4 h.

The cyclic voltammograms (CVs) of the catalysts were obtained using a conventional three-electrode cell described previously [43] using a potential sweep rate of 10 $mV \cdot s^{-1}$. A small quantity of the catalyst powder (0.002 g approximately) was pressed onto a platinum mesh to form the working electrode. All the CV experiments were performed at ambient temperature (around 25 °C) and a palladium wire charged with hydrogen and contained within the electrolyte was used as a reference electrode. The working electrolyte (0.5 M H_2SO_4) was deaerated by bubbling nitrogen through the solution for at least 30 min before running CV. CO adsorption was carried out by placing the working electrode in a CO bubbler for set periods of time to vary CO coverage. The electrode with CO adsorbed was then immediately transferred into the electrochemical cell (protected by a CO saturated droplet of water) and contacted with the electrolyte at a potential of 0.05 V versus Pd/H and a CV of the CO stripping peak collected.

X-ray photoelectron spectroscopy (XPS) measurements were performed on an ESCA300 (Scienta) spectrometer based at the Synchrotron Radiation Source at Daresbury Laboratories, UK. For Pt and Rh element surveys, the pass energy was set as 150 eV, the step energy was set as 0.05 eV and the time per step was 0.1 s.

Table 1
Calculated monolayer equivalents for the fresh catalysts.

Volume of $RhCl_3$/ml	5% Pt/G area/m^2 A	Rh adlayer area/m^2 B	Rh coverage/ML B/A
0.2	0.4255	0.0638	0.15
0.4	0.3645	0.1277	0.35
0.8	0.3928	0.2554	0.65
1.2	0.3429	0.3830	1.12
1.5	0.3628	0.4788	1.32
1.8	0.3467	0.5746	1.66
2.0	0.3345	0.6384	1.91
4.0	0.3425	1.2768	3.73
6.0	0.3880	1.9152	4.94
12.0	0.3309	3.830	11.57

c (Rh^{3+}): 0.0094 mol/l, ML = monolayer equivalent radius of Rh 1.34 × 10^{-10} m, 5% Pt/G surface area is 2.1 m^2/g for fresh and 1.0 m^2/g after heating in 5% hydrogen/95% argon mixture at 700 K for 4 h.

3. Results and discussion

3.1. Growth of rhodium adlayers on 5% Pt/G substrates and CO oxidation

3.1.1. CV characterisation of Rh_x/5% Pt/G (not annealed)

Fig. 1 shows CVs of the freshly prepared Rh_x/5% Pt/G catalysts (the x value varying from zero to approximately 2 monolayer equivalents). The potential ranges around the principal Rh hydrogen underpotential deposition (H UPD) (Fig. 1(a)) and Pt H UPD (Fig. 1(b)) peaks are expanded for clarity. It is seen that on the positive-going scan, a peak

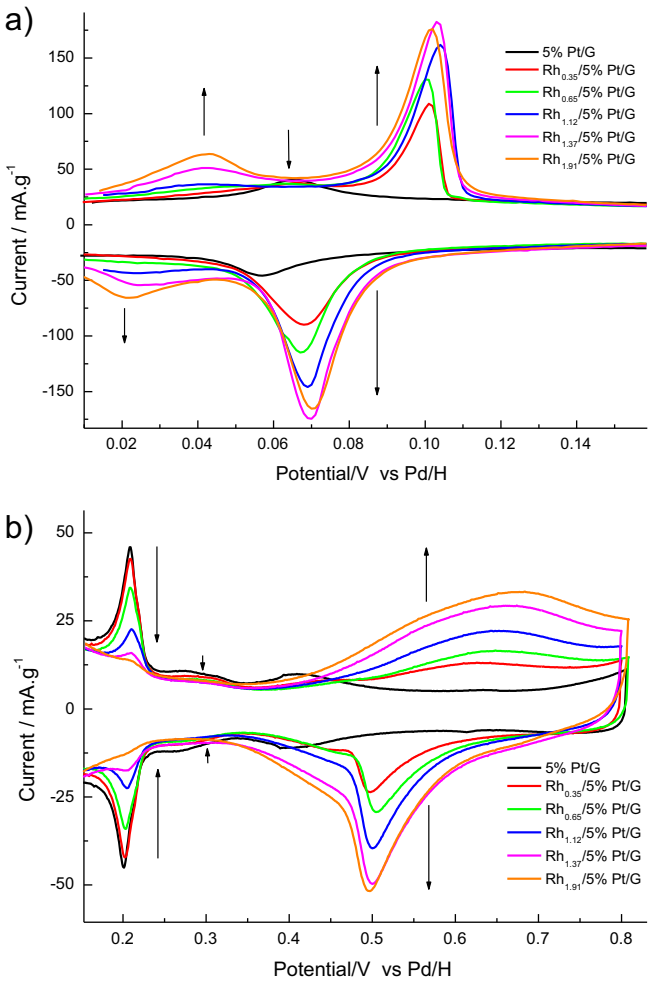

Fig. 1. (a) and (b) are expanded CV profiles of fresh Rh_x/5% Pt/G for 0 < x < 2 monolayer equivalents. Test solution: 0.5 M H_2SO_4. Sweep rate: 10 mV·s^{-1}.

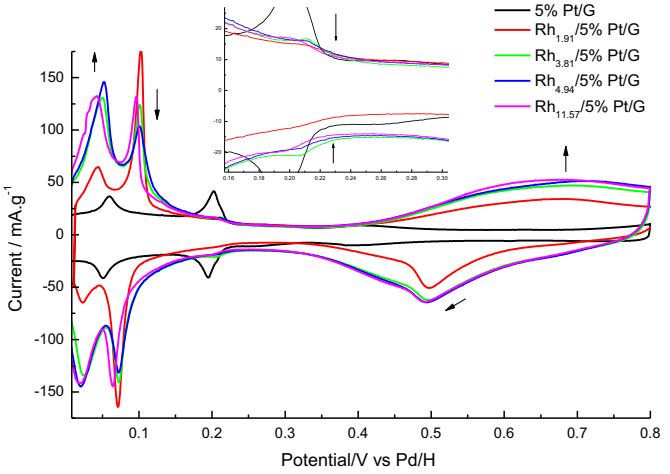

Fig. 2. CV profiles of fresh Rh_x/5% Pt/G (1.9 < x < 12 monolayer equivalents). The insert is the expansion of the Pt(100)x(111) step H UPD region. Test electrolyte: 0.5 M H_2SO_4. Sweep rate: 10 mV·s^{-1}.

first appears at 0.10 V ascribable to first layer Rh followed quickly (x > 0.65) by the appearance of a second Rh feature at 0.042 V associated with the commencement of second and third layer Rh growth [5]. It is also apparent that the second Rh peak appears before the first reaches its maximum intensity consistent with multilayer growth of Rh occurring before all Pt sites are covered by Rh. The attenuation of the Pt {100}x{111} step peak at 0.2 V by only 30–40% at this stage also supports this assertion that Rh does not wet completely the Pt catalyst surface but rather forms microcrystallites at submonolayer equivalents of Rh loading. This growth behaviour is consistent with previous single crystal studies of Rh on Pt [5,24,33,34,44] and the Rh coverage at which deviation from Frank-van der Merwe growth occurs is also remarkably consistent with previous studies [2]. Hence, our coverage estimations based on "equivalent monolayers" appear sound and moreover suggest that all Rh (at least initially) is deposited on metal sites only. If Rh deposition was occurring on graphite, the magnitude of the Rh H UPD peak at 0.042 V together with its peak width would have to be much larger than reported here. Later, XPS will be used to show that bulk Rh on graphite is unlikely to be forming at submonolayer Rh coverages. In addition to the relative areas of the Rh H UPD peaks, inspection of the electrochemical oxide states (Fig. 1(b)) shows that the initial deposits of Rh lead to the generation of two Rh oxide stripping features on the negative-going scan and a regular increase in total oxide peak area as Rh loading is increased systematically. The first oxide stripping peak at 0.5 V is rather narrow and is larger in magnitude than the shoulder situated at more negative potential (0.4 V). The ratio of intensities between the two peaks changes as Rh loading increases such that in Fig. 2, it is evident that the sharp peak at 0.5 V becomes the minority species compared to the shoulder. Hence, we ascribe the shoulder peak at more negative potentials to stripping of electrochemical oxide from "rough, defective" Rh microcrystallites (Rh coverage > 1 monolayer) which clearly increase in number as Rh coverage increases (see also Fig. 2 Rh H UPD peak at 0.042 V which grows in intensity at the expense of the H UPD peak associated with first layer Rh). We estimate that the Rh 1st layer peak goes through a maximum at 1.9 monolayer equivalents just as the last Pt sites become occupied (see Fig. 1(b) Pt H UPD peak at 0.2 V which is attenuated completely at this coverage).

The ratio of total H UPD charge at x = 0 compared to x = 12 indicates a roughness factor of 4–5 for the highest Rh loading catalyst compared to the pristine 5% Pt/G catalyst.

3.1.2. XPS characterisation of Rh_x/5% Pt/G (not annealed)

X-ray photoelectron spectra of the Rh 3d and Pt 4f regions for fresh Rh_x/5% Pt/G catalysts are presented in Fig. 3(a) and (b) respectively together with a 5% Rh/G catalyst (curve f in Fig. 3(a)) prepared by reduction of $RhCl_3$(aq) onto graphite in a hydrogen bubbler (identical to the method used to prepare PtRh bimetallic catalysts). The XP spectrum of the 5% Rh/G material showed Rh 3d peaks at 309.4 and 314.1 eV (strong, attributed to Rh^{3+} in un-reduced Rh_2O_3) and at 307.3 and 312.0 eV (weaker, for Rh^0 in Rh metal). XPS survey scans confirmed the absence of chlorine at 199 eV binding energy although strong peaks did appear (in addition to Rh peaks) at binding energies of 530 eV (oxygen) and 284 eV (graphite) and thus confirmed that the Rh deposit was largely present as the oxidised phase on graphite. By contrast, all samples of Rh/Pt/graphite and (Pt + Rh + Pt)/Pt/graphite (see later) provide spectra containing peaks at 307.3 and 312.0 eV for metallic Rh^0 and a weak peak at 308.4 eV for Rh^{1+}. Hence, Rh on graphite is readily distinguishable from Rh adsorbed on 5% Pt/G in that Rh^{3+} XPS peaks associated with "bulk" Rh are completely absent. We suggest that the loadings of Rh used in the present study are sufficiently low to prevent deep oxidation of Rh due to the proximity of the more noble Pt component.

The relative areas of the Rh $3d_{5/2}$ and Pt $4d_{5/2}$ peaks as a function of metal loading (for 0 < x < 1) are in good agreement with previous XPS coverage determinations by Tanaka et al. [45] who studied evaporated Rh films on Pt{100} by LEED/XPS. The only difference between the XPS peaks reported in our study and those by Tanaka and co-workers is that both Rh^{1+} and Rh^0 species are present in the Rh modified 5% Pt/G catalyst in comparison with pure metallic Rh, the XPS features of which were reported in the earlier UHV study. We also simulated variations in XPS peak magnitudes for Rh 3d, Pt 4d and Pt 4f as a function of depositing complete 1st, 2nd and 3rd Rh layers using the NIST Database

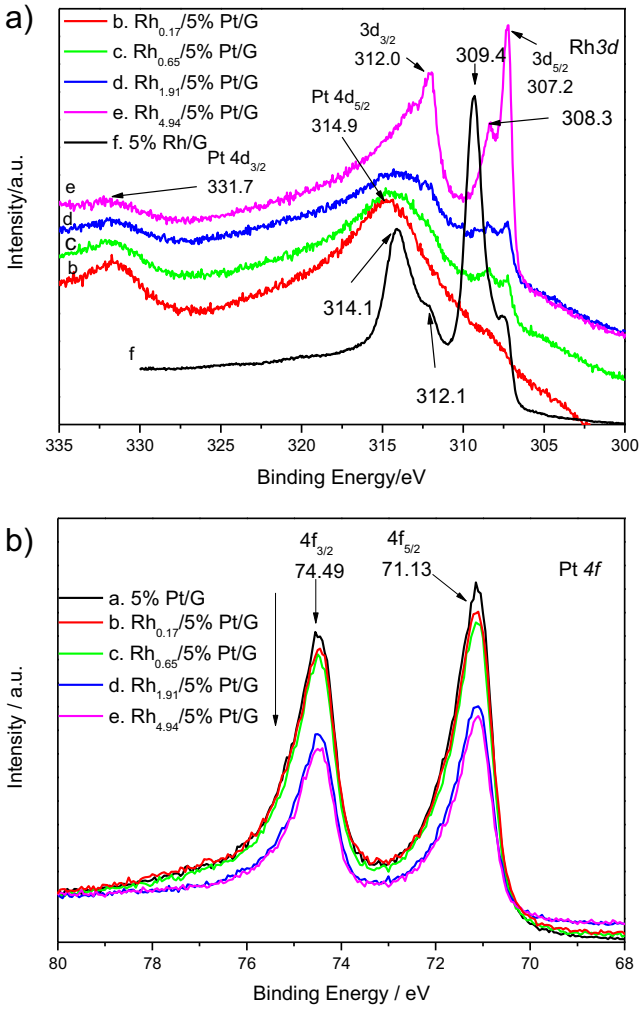

Fig. 3. X-ray photoelectron spectra of (a)—Rh 3d and (b)—Pt 4f regions for fresh Rh_x/5% Pt/G. The values of x are: a. 0.00, b. 0.17, c. 0.65, d. 1.91, and e. 4.94. In (a) curve f. corresponds to a 5% Rh/G catalyst.

for the Simulation of Electron Spectra for Surface Analysis (SESSA) software [46]. It was evident from these simulations that the predicted attenuation in Pt 4d and 4f peaks after 3 monolayers of Rh did not match experiment in that an almost 55% decrease in Pt 4f signal would be predicted whereas for a $x = 4.94$ equivalent monolayers, the 4f peak is only attenuated to approximately 60% of its original value. Hence, XPS also confirms deductions from CV that the Rh is not growing via a simple layer-by-layer mechanism but rather is deviating strongly from this growth mode at high metal loadings. Nonetheless, the congruence between Rh coverage determined using CV/XPS/equivalent monolayers (at least for $0 < x < 1$) and growth mode using CV and XPS supports the notion that very little Rh is nucleating at the graphite support and that most is adsorbing at the Pt metal sites when using hydrogen as the reducing agent. From Fig. 3(b), the binding energy of the Pt $4f_{7/2}$ peak remains unchanged as x increases indicating emission from the underlying Pt phase is not influenced by Rh deposition. Later, it will be demonstrated that changes in the binding energy of the Pt $4f_{7/2}$ peak occur when alloying with Rh takes place. Hence, we assert that no intermixing of Rh with Pt takes place at room temperature consistent with both our earlier studies [2] and Tanaka et al. [45]. The changes in relative intensity between the $3d_{5/2}$ 307.2 eV and 308.4 eV peaks as a function of increasing Rh loading are consistent with corresponding changes in the ratio of surface to bulk rhodium atoms. At low values of x, it is expected that for small microcrystallites, the number of surface sites to bulk is similar. However, as these microcrystallites grow in volume, the ratio of surface atoms to bulk atoms would decrease. Hence, we ascribe the Rh $3d_{5/2}$ 308.4 eV peak at higher binding energy to surface Rh atoms bonded to chemisorbed oxygen and the feature at 307.2 eV to bulk, fully reduced rhodium.

3.1.3. CO electrooxidation on fresh Rh_x/5% Pt/G

Fig. 4 presents CO stripping profiles of freshly prepared Rh_x/5% Pt/G samples with x values of 0, 0.35, 0.65, 1.6 and 4.94 respectively. For the different samples, CO oxidation has been studied for different initial CO coverages by holding the electrode in a CO bubbler for greater and greater exposure times. For the 5% Pt/G catalyst, a single CO stripping peak is observed at 0.71 V when 60% of H UPD sites are blocked by CO. As CO initial coverage increases to 90% of H UPD sites blocked, a second shoulder peak begins to appear. At full blocking of H UPD sites, this small shoulder peak develops still further but the majority peak shifts to 0.72 V. All CO stripping peaks lie within the envelope defined by the highest CO coverage. When Rh is deposited onto the catalyst (Fig. 4(b–d)), increasing the CO dosing leads to both CO electrooxidation onset potential and peak potential shifting to more positive values whilst the leading edge of the stripping peaks does not overlap, i.e. a portion of the low potential CO stripping peak always lies outside of the envelope defined by the highest coverage CO electrooxidation peak. We suggest that this phenomenon which evidently distinguishes Rh sites from Pt sites is associated with competition for sites between CO and electrochemical Rh oxide formation, the onset of which occurs negative of the onset of CO stripping at the highest CO coverage but almost coincides for low CO dosing. Hence, high coverage of CO inhibits Rh electrochemical oxide formation. This behaviour is not found with Pt since its electrochemical oxide formation potential lies at a more positive potential than Rh and therefore competition with CO for adsorption sites is much reduced. Later, it will be shown that PtRh alloys disfavour electrochemical oxide formation at these low potentials and thus all CO stripping peaks lie within the envelope of the highest CO coverage stripping peak as found with pure Pt. In addition to changes induced in the overall CO stripping profile by Rh, the number of stripping peaks is closely correlated with the amount of first layer/multilayer Rh adsorbed. For example, looking at Fig. 4(b–c) it is evident that as the intensity of the Rh H UPD peak at 0.042 V increases, so too does a CO electrooxidation peak situated at 0.6 V, some 80 mV negative of CO stripping from first layer Rh. Another distinguishing feature of CO electrooxidation on 5% Pt/G compared with Rh_x/5% Pt/G is the marked increase in peak fullwidth at half maximum which changes from 60 mV in the former to 110 mV for the latter. Hence, the electrocatalytic activity for CO electrooxidation may readily be distinguished on Pt and Rh sites and follows the order:

$$\mathrm{Rh(multilayer\,0.60\,V) > Rh(monolayer\,0.68\,V) > Pt(0.72\,V).}$$

The shift in CO stripping peak potential as a function of increasing CO coverage may be interpreted within a “bi-functional mechanism” [47] whereby Rh initially adsorbs OH at a lower potential than Pt thus CO is preferably oxidised firstly on the 1st Rh monolayer or the edge of Rh small islands at low CO dosings. At higher CO coverages, diffusion of either CO or OH is inhibited thus leading to an increase in the overpotential for CO electrooxidation.

3.2. Thermally treated Rh_x/5% Pt/G, CO oxidation and XPS characterisation

3.2.1. CO stripping on thermally treated Rh_x/5% Pt/G

In a previous study, it was found that gentle flame annealing of a Rh deposit on a Pt{100} single crystal electrode led to the formation of PtRh surface alloys [5]. Therefore, in order to replicate this procedure and hopefully generate alloyed surfaces, two Rh on Pt samples ($Rh_{1.5}$/5% Pt/G and $Rh_{4.94}$/5% Pt/G) were heated in a flow of 5% H_2/Ar at 700 K for 4 h (Fig. 5(a) and (b) respectively) and their voltammetry compared with the unannealed samples. The data corresponding to the unannealed

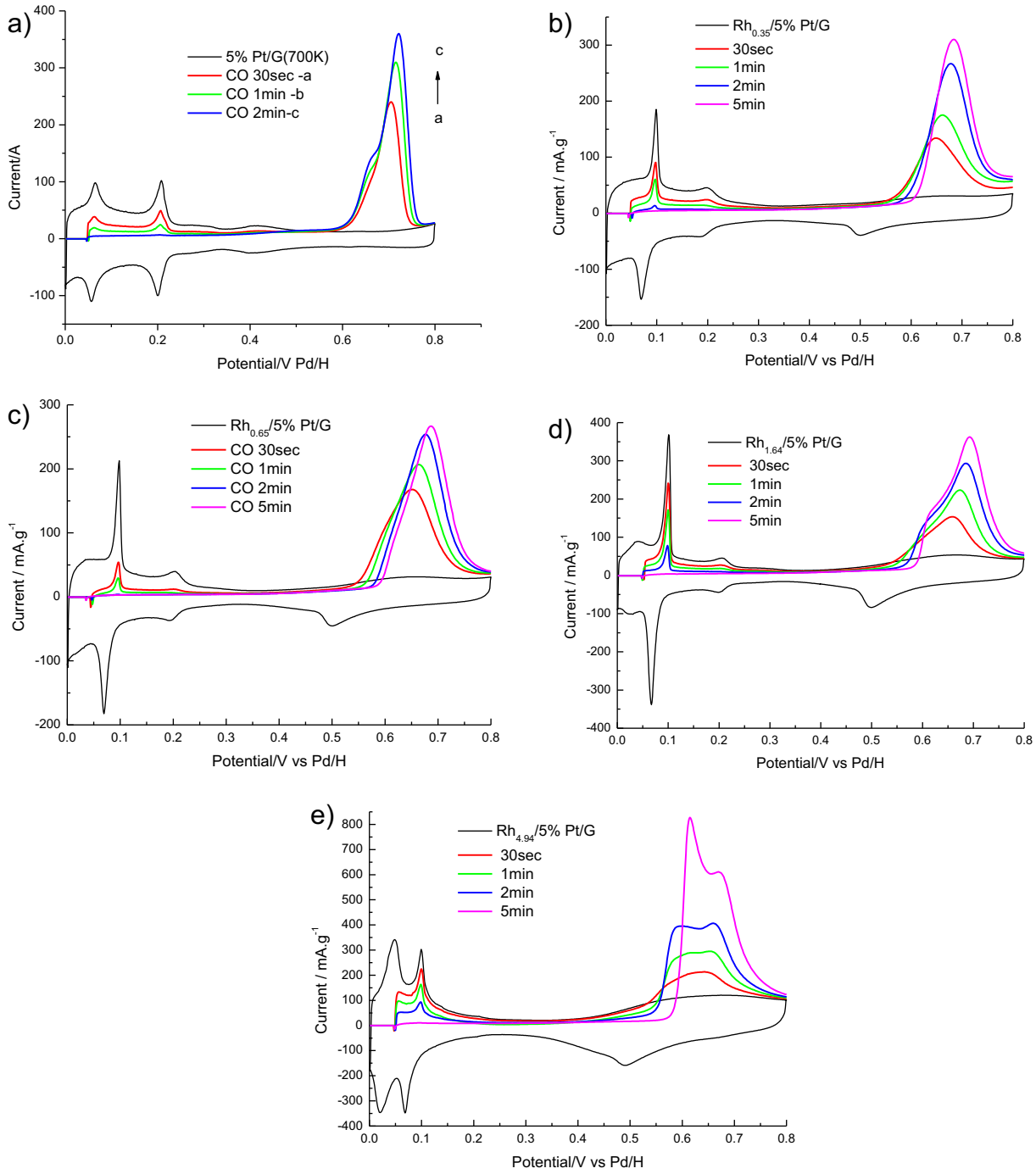

Fig. 4. Voltammetric profiles of CO oxidation on fresh (a) 5% Pt/G; (b) $Rh_{0.35}$/5% Pt/G; (c) $Rh_{0.65}$/5% Pt/G; (d) $Rh_{1.5}$/5% Pt/G and (e) $Rh_{4.94}$/5% Pt/G. Test electrolyte: 0.5 M H_2SO_4. Sweep rate: 10 mV·s^{-1}. 30 s, 1, 2 and 5 min indicate CO adsorption time before running CO stripping CV.

samples are also shown in Fig. 5. It is evident that thermal annealing leads to a decrease in total H UPD charge suggesting that the overall roughness factor (relative to 5% Pt/G) is decreased significantly. In addition, from Fig. 5(a), the 0.09 V Rh peak is reduced to approximately 5% of its original value although a new peak appears at 0.05 V, just positive of the Rh multilayer state. Although the potential of the 0.09 V peak is similar to where the clean Pt{111}x{111} step feature is expected, we discount this being a purely Pt peak because Fig. 5(b) shows that this peak reaches a much greater magnitude than expected for clean 5% Pt/G (see Fig. 4(a)), particularly in relation to the Pt{100}x{111} peak at 0.2 V. Rather, we ascribe the changes highlighted above to intermixing of Rh into the selvedge of the 5% Pt/G surface with a commensurate increase in surface Pt population. From UHV studies [2,45] it is fully expected that Rh should diffuse into the bulk upon annealing and we suggest that this is where the "lost" overlayer Rh resides. Another striking feature of the annealed samples is the substantial loss of Rh oxide charge and the shift to more positive potentials in its onset after thermal treatment. This is particularly pronounced in Fig. 5(b) where Rh oxide formation commences at 0.35 V for unannealed catalyst but shifts to 0.57 V after thermal treatment. That Rh is still present in the surface of the catalyst may be gleaned from the magnitude and position of the oxide stripping peak at 0.48 V and the residual H UPD peaks at 0.09 V (much sharper than in the unannealed surface but here assigned to Rh overlayer on top of either Pt or Pt-rich PtRh surface alloy) at 0.05 V (a new peak which we ascribe to H UPD

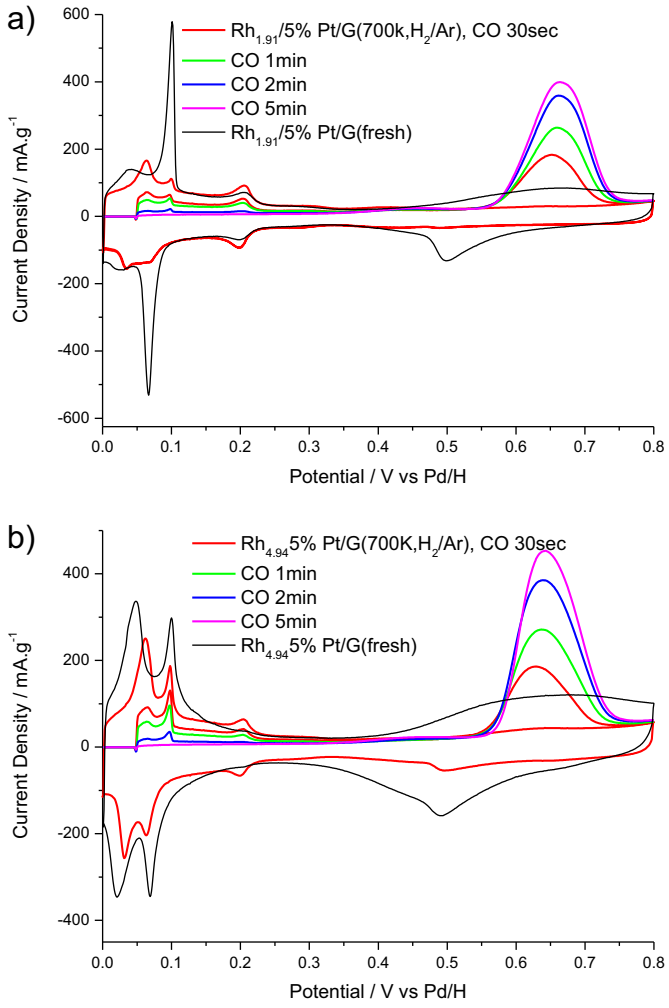

Fig. 5. CO stripping profiles on Rh_x/5% Pt/G after heating in 5% H_2/Ar at 700 K for 4 h, (a) $Rh_{1.5}$/5% Pt/G; (b) $Rh_{4.94}$/5% Pt/G. Electrolyte: 0.5 M H_2SO_4. Sweep rate: 10 $mV \cdot s^{-1}$. 30 s, 1, 2 and 5 min indicate CO adsorption time before obtaining the CV.

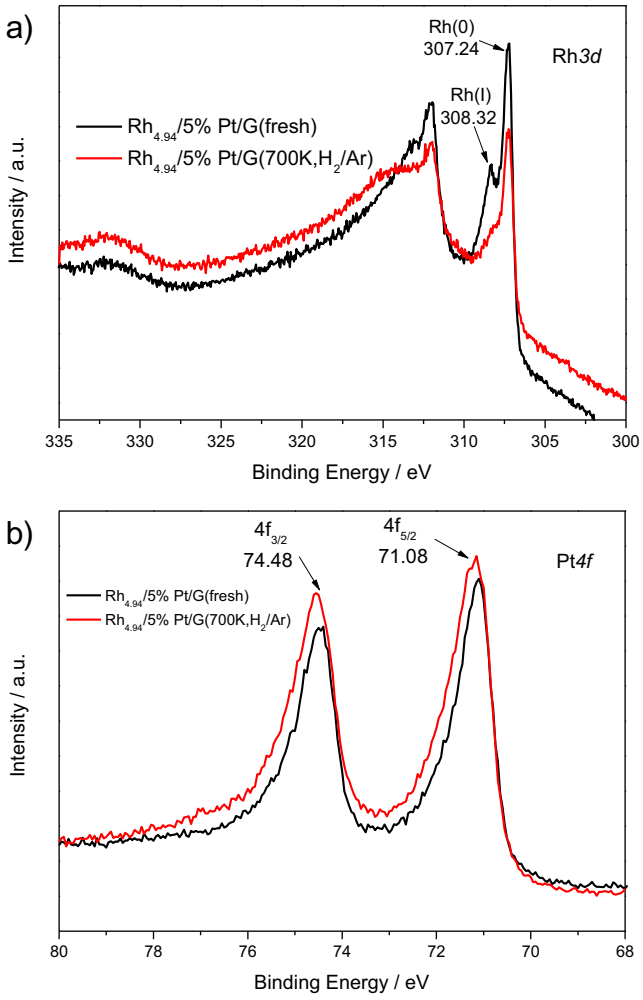

Fig. 6. X-ray photoelectron spectra of (a)—Rh 3d and (b)—Pt 4f regions in fresh and annealed (700 K H_2/Ar mixture) Rh_x/5% Pt/G.

on Rh-rich alloy due to its proximity to the Rh multilayer peak potential). The corresponding CO stripping peaks from the thermally treated catalysts are in line with expectations in that because the electrochemical oxide phase now forms at more positive potentials than before, CO oxidation (removal) does not inhibit oxide formation so all CO stripping peaks fall within the envelope of the highest coverage stripping peak. The peak potential from the intermixed PtRh phase lies between 0.62 and 0.65 V depending on CO coverage but clearly lies significantly more negative in potential than for clean Pt. In the next section, we use XPS to interrogate changes in the Rh_x/5% Pt/G catalysts when heated in the presence of flowing hydrogen gas and compare these changes with CV.

3.2.2. XPS characterisation of PtRh phases prepared by heating Rh_x/5% Pt/G

Fig. 6 shows XPS data for a $Rh_{4.94}$/5% Pt/G sample before and after thermal treatment in flowing 5% H_2/95% Ar at 700 K. Comparing the Rh 3d peaks for both catalysts, it is apparent that a diminution in peak intensity occurs following annealing consistent with the earlier CV results highlighted in Fig. 5(b). This behaviour together with the increase in the magnitudes of the Pt 4f XPS peaks is consistent with diffusion of Rh into the underlying Pt phase. Further support for intermixing of Rh and Pt may be obtained from consideration of a small, but reproducible shift of 0.1 eV to higher binding energies of the 4f Pt XPS peaks upon annealing the Rh adlayer. It should be remembered that no shift in binding energy was recorded for the unannealed adlayer, irrespective of Rh coverage. Another facet of the thermally treated catalyst is the very low intensity afforded by the Rh^{1+} XPS feature after heating compared to fresh $Rh_{4.94}$/5% Pt/G. This indicates that the surface is more resistant to oxidation, i.e. it is more noble (like Pt) in agreement with findings obtained using CV. Hence, it is concluded based on the loss of Rh from the X-ray photoemission spectrum, the inhibition of surface oxidation and especially the shift in Pt 4f binding energy that a RhPt alloy phase has been formed following thermal treatment [5].

3.3. PtRh surface alloy prepared by heating $Pt_xRh_yPt_z$/Pt_5/C sandwich structures

It was demonstrated in Ref. [5] that heating a sandwich structure containing alternate layers of Pt/Rh/Pt adsorbed on Pt{100} afforded the most efficient generation of PtRh alloy phases. In what follows, this procedure is used to generate PtRh alloys having various compositions.

3.3.1. CVs of PtRh surface alloy phases derived from $Pt_xRh_yPt_z$/Pt_5/C sandwich structures

Fig. 7 shows the CVs of a series of $Pt_xRh_yPt_z$/5% Pt/G sandwich structures that have been thermally annealed at 700 K in hydrogen/argon with different amounts x, y, and z of Pt and Rh. According to the growth in the intensity of the electrochemical oxide phase, the amount of Rh in the surface after annealing varies as follows:

$$Pt_{0.38}Rh_{1.91}Pt_{0.38}(A) < Pt_{2.4}Rh_{11}Pt_{2.4}(B) < Pt_1Rh_{11}Pt_1(C) < Pt_{0.38}Rh_8Pt_{0.38}(D)$$

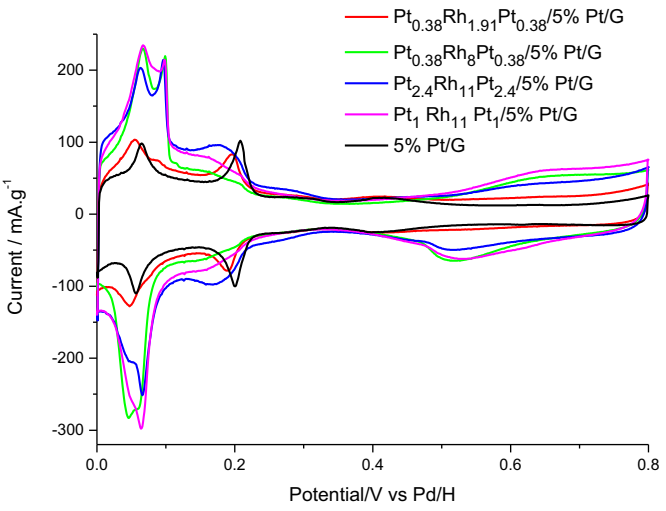

Fig. 7. CVs of $Pt_xRh_yPt_z$/5% Pt/G sandwich-like catalysts annealed at 700 K in H_2/Ar where x, y and z are amounts of Rh or Pt in monolayer equivalents. The continuous line corresponds to 5% Pt/G. Electrolyte solution: 0.5 M H_2SO_4. Sweep rate: 10 $mV \cdot s^{-1}$.

where A–D is used as a shorthand for the different bimetallic phases formed.

It is noteworthy that in comparison with simple Rh overlayers, the electrochemical oxide region exhibits both a lower overall magnitude and the onset of oxidation takes place at more positive potentials. Both of these aspects suggest that surface alloys have been produced since the surface of the electrode now resists surface electrochemical oxidation. However, it is when detailed analysis of changes in the H UPD region is undertaken that it becomes apparent that electrosorption peaks characteristic of neither clean Pt nor Rh adlayers are now observed. For example, for alloy A, although ostensibly very similar to the 5% Pt/G CV profile, subtle shifts to more negative potentials in both of the Pt step peaks at approximately 0.05 and 0.2 V indicate the presence of Rh. For alloys B–D, the H UPD region between 0 and 0.1 V corresponds to Rh rich phases. As found in Fig. 5, two peaks are observed, one very narrow situated at 0.09 V reminiscent of excess Rh adlayer bonded to Pt and a slightly broader peak at more negative potentials (0.05 V) that we ascribe to a Rh-rich alloy phase. Between 0.1 V and 0.2 V is seen a very broad H UPD region that should be associated (by virtue of its potential range) with Pt rich sites. Therefore we ascribe this potential range to Pt-rich PtRh alloy phase. According to CV, this range of potential is most intense for alloy B and this is consistent with using the highest amount of Pt in the sandwich structure (2.4 monolayer equivalents in each layer). In fact the ratio of Pt/Rh in terms of equivalent monolayers laid down for catalysts A–D is 0.4, 0.44, 0.1818 and 0.095 respectively and so it is interesting to compare this broad "prediction" of changes in the ratio of Pt/Rh and the actual experimental results. Clearly catalyst A is largely a Pt like surface so most of the Rh has diffused into the bulk. Yet for catalysts B–D, the trend in the ratio of Pt/Rh predicted above agrees well with the sequence of decreasing Pt-rich alloy H UPD charge between 0.1 and 0.2 V and increasing magnitude of the H UPD peak associated with the Rh-rich alloy phase at 0.05 V going from B to D.

3.3.2. XPS characterisation of PtRh surface alloys derived from $Pt_xRh_yPt_z$/5% Pt/G sandwich structures

In Fig. 8, both the ratio of peak intensities between the Pt $4d_{5/2}$ and the Rh $3d_{3/2}$ XPS peaks and the relative decrease in 4f intensity indicate that the amount of Rh in the surface follows the order (using the same 'shorthand' nomenclature above for each of $Pt_xRh_yPt_z$ sandwich structures above) A < B < C < D. This is in exact agreement with predictions made using CV and the ratio of Pt/Rh comprising the sandwich structure. A remarkable result is clearly observed whereby the Rh^{1+} $3d_{5/2}$ peak at 308.3 eV is hardly visible for any of the heated sandwich structures. Rather, the surface of the metal particles consists almost entirely of Rh in its zero oxidation state as revealed by the relative magnitude (compared to the 308.3 eV signal) of the 307.2 eV Rh $3d_{5/2}$ peak. This again confirms that the rhodium–platinum selvedge region is much more resistant to oxidation once annealed (as found also with CV analysis). In a paper by Somorjai et al. [48], XPS was used to analyse the composition of a series of well-defined PtRh alloy nanoparticles. Using their data and calibration curve whilst observing changes in the relative intensities of the Pt 4d, Rh 3d and Pt 4f XPS peaks as a function of composition, we find that our alloy compositions are approximately:

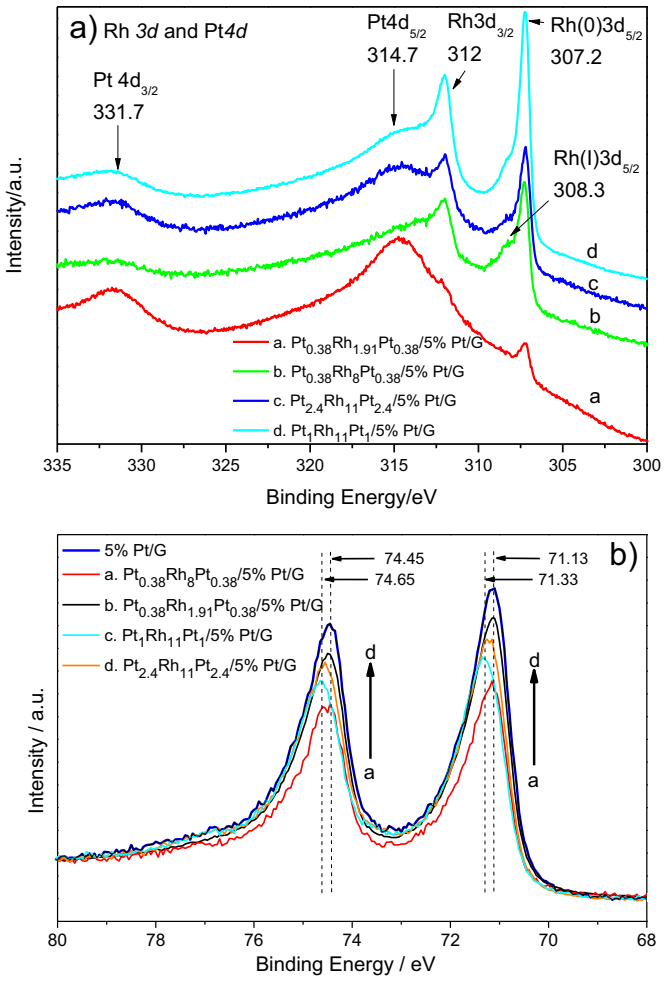

Fig. 8. X-ray photoelectron spectra of (a)—Rh 3d and (b)—Pt 4f regions for catalysts derived from heating sandwich-like deposits of $Pt_xRh_yPt_z$ at 700 K in 5% H_2/Ar.

$$A(10\%Rh) < B(30\%Rh) < C(40\%Rh) < D(50\%Rh).$$

This evaluation of alloy composition has to be taken with some caution however because the calibration work upon which composition determination was based assumed a homogeneous distribution of Pt and Rh in the non-thermally equilibrated nanoparticle alloy whereas in our case, it may be that some heterogeneity in the selvedge region associated with preferential segregation of one or other component is occurring [49]. Pt $4f_{3/2}$ and Pt $4f_{5/2}$ peaks are seen to shift to approximately 0.2 eV higher binding energies for two of the sandwich structures, namely $Pt_1Rh_{11}Pt_1$ (C) and $Pt_{2.4}Rh_{11}Pt_{2.4}$ (B) suggesting an alloy has formed here sufficient to perturb the majority of Pt atoms in the selvedge away from their pure Pt binding energy values. This finding would support our contention that the H UPD electrosorption charge between 0.1 and 0.2 V discussed in Fig. 7 is consistent with a Pt-rich PtRh surface

alloy phase. It is interesting however that both the $Pt_{0.38}Rh_{1.91}Pt_{0.38}$ (A) and $Pt_{0.38}Rh_8Pt_{0.38}$ (D) bimetallic surfaces show no shift in Pt 4f binding energy. Both show the weakest H UPD charge contribution between 0.1 and 0.2 V in their CV suggesting that the BE shift is associated only with a Pt-rich PtRh alloy phase.

3.3.3. CO stripping on PtRh surface alloys derived from $Pt_xRh_yPt_z$/5% Pt/G sandwich structures

As discussed in Section 3.2.1, CO electrooxidation on PtRh surface alloys displays quite different stripping peak behaviour compared with simple Rh adlayers due to variations in their propensity to form electrochemical oxides. After heating $Pt_xRh_yPt_z$ sandwich structure deposits in 5% H_2/Ar at 700 K for 4 h, CO electrooxidation behaviour is consistent with the presence of more oxide resistant adsorption sites as shown in Fig. 9(a, b, c and d) for $Pt_{0.38}Rh_{1.91}Pt_{0.38}$/5% Pt/G, $Pt_{0.38}Rh_{1.85}Pt_{0.38}$/5% Pt/G, $Pt_{2.4}Rh_{11}Pt_{2.4}$/5% Pt/G and $Pt_1Rh_{11}Pt_1$/5% Pt/G, respectively.

A close inspection of the CV results (Fig. 9) reveals that the most negative shift from the clean Pt value of the CO stripping peak corresponds to the two Pt-rich surface alloy phases Pt_1Rh_{11} Pt_1/5% Pt/G and $Pt_{2.4}Rh_{11}P_{.2.4}$/5% Pt/G with the former being the most active with a potential centred at 0.59 V some 120 mV lower than clean Pt. In addition, the onset of CO electrooxidation on both of these bimetallic surfaces is found to be approximately 0.25–0.3 V which is much lower than for any of the Rh overlayers discussed in Fig. 4 and suggests a useful role for such alloys as CO-tolerant alloys for use as fuel cell anodes. These findings are in accord with previous measurements of CO electrooxidation on PtRh{100} surface alloys [5].

4. Conclusion

CV and XPS have been used to study novel bimetallic RhPt phases supported on 5% Pt/G. For freshly prepared Rh adlayers, both CV and XPS characterisations show that Rh does not grow in a simple layer by layer fashion. Rather, the second and subsequent Rh monolayers commence growing before first Rh monolayer is complete. It is concluded that preferential deposition of aqueous Rh^{3+} ions on platinum takes place compared to graphite when hydrogen is used as the reducing agent. For CO monolayer electrooxidation experiments on Rh adlayers as a function of increasing CO dosing, both CO onset potential and peak potential shift to more positive values whilst the leading edges of the stripping peaks do not overlap. At highest Rh loadings, CO electrooxidation gives rise to two independent CO oxidation peaks, one at more positive potential for CO oxidation on first monolayer Rh and one at more negative potential on Rh multilayers on Pt. PtRh surface alloys formed by heating Rh_x/5% Pt/G catalysts in 5% H_2/Ar at 700 K display a remarkably different CO electrooxidation response compared to

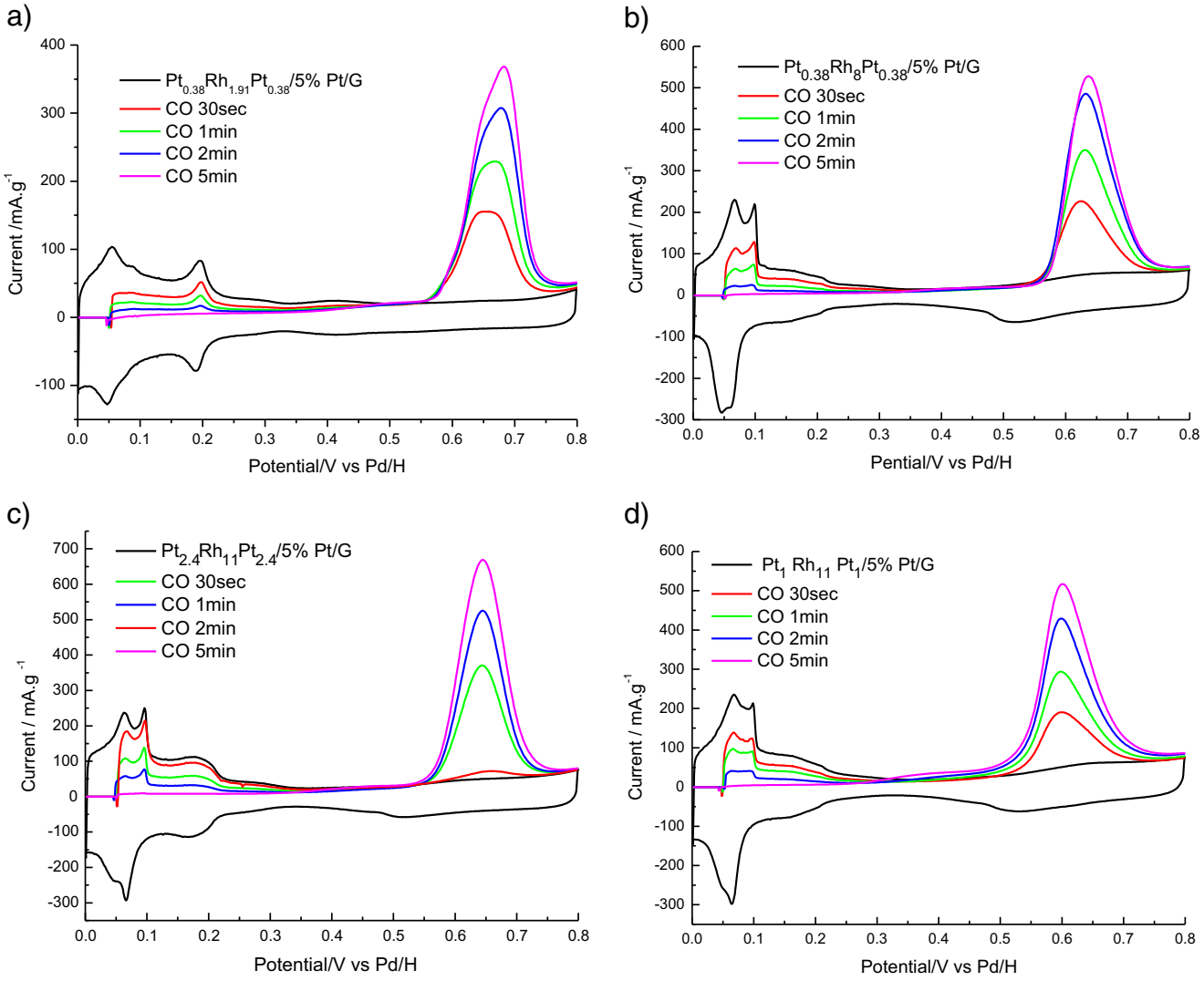

Fig. 9. Voltammetric profiles of CO stripping on: (a) $Pt_{0.38}Rh_{1.91}Pt_{0.38}$/5% Pt/G, (b) $Pt_{0.38}Rh_8Pt_{0.38}$/5% Pt/G, (c) $Pt_{2.4}Rh_{11}P_{.2.4}$/5% Pt/G and (d) Pt_1Rh_{11} Pt_1/5% Pt/G after heating at 700 K in 5% H_2/Ar. Solution: 0.5 M H_2SO_4. Sweep rate: 10 mV·s^{-1}.

fresh Rh deposits in that all CO stripping peaks, irrespective of CO coverage, lie within the stripping envelope defined by the maximum CO coverage.

It has also been shown that PtRh surface alloys may be prepared by heating either the fresh Rh adlayer deposit or a sandwich structure consisting of alternate Pt/Rh/Pt layers in hydrogen. The presence of a PtRh alloy was deduced using CV and XPS and in particular, the Pt rich bimetallic phase resulted in a small but reproducible binding energy shift to larger values in the Pt 4f XPS peaks. Alloys that gave rise to this binding energy shift also proved to be the most active for CO electrooxidation. A nominal optimal alloy composition between 30 and 40% appears best for electrocatalytic oxidation of CO using a calibration curve first published in Ref. [48]. The results are consistent with those obtained for PtRh{100} and previously reported [5].

Future studies will employ still higher Rh loadings since single crystal studies indicate a potential electrooxidation capability of surface PtRh alloys (upon which are deposited Rh islands) as low as 0.45 V Pd/H, comparable with certain Ru alloys. More importantly, Rh is less susceptible to leaching than Ru.

Acknowledgments

The authors would like to thank the EPSRC (EP/D06015X/1) for the financial support. Li Fang also acknowledges the financial support of Shanxi Scholarship Council of China.

References

[1] G.A. Attard, R. Price, Surf. Sci. 335 (1-3) (1995) 63.
[2] G.A. Attard, R. Price, A. AlAkl, Surf. Sci. 335 (1–3) (1995) 52.
[3] F.J. Vidal-Iglesias, J. Solla-Gullon, E. Herrero, A. Aldaz, J.M. Feliu, Angew. Chem. Int. Ed. 49 (39) (2010) 6998.
[4] F.J. Vidal-Iglesias, A. López-Cudero, J. Solla-Gullón, J.M. Feliu, Angew. Chem. Int. Ed. 52 (3) (2013) 964.
[5] L. Fang, F.J. Vidal-Iglesias, S.E. Huxter, G.A. Attard, J. Electroanal. Chem. 622 (1) (2008) 73.
[6] F.J. Vidal-Iglesias, A. Al-Akl, D. Watson, G.A. Attard, J. Electroanal. Chem. 611 (1–2) (2007) 117.
[7] F.J. Vidal-Iglesias, A. Al Akl, D.J. Watson, G.A. Attard, Electrochem. Commun. 8 (7) (2006) 1147.
[8] S.E. Huxter, G.A. Attard, Electrochem. Commun. 8 (11) (2006) 1806.
[9] T.J. Schmidt, V. Stamenkovic, G.A. Attard, N.M. Markovic, P.N. Ross, Langmuir 17 (24) (2001) 7613.
[10] T.J. Schmidt, N.M. Markovic, V. Stamenkovic, P.N. Ross, G.A. Attard, D.J. Watson, Langmuir 18 (18) (2002) 6969.
[11] W.H. Lizcano-Valbuena, D.C. de Azevedo, E.R. Gonzalez, Electrochim. Acta 49 (8) (2004) 1289.
[12] J.S. Spendelow, A. Wieckowski, Phys. Chem. Chem. Phys. 6 (22) (2004) 5094.
[13] N.M. Markovic, P.N. Ross, Surf. Sci. Rep. 45 (4–6) (2002) 117.
[14] G.Q. Lu, P. Waszczuk, A. Wieckowski, J. Electroanal. Chem. 532 (1–2) (2002) 49.
[15] H.N. Dinh, X. Ren, F.H. Garzon, Z. Piotr, S. Gottesfeld, J. Electroanal. Chem. 491 (1–2) (2000) 222.
[16] L. Dubau, F. Hahn, C. Coutanceau, J.M. Léger, C. Lamy, J. Electroanal. Chem. 554–555 (1) (2003) 407.
[17] A. Pozio, R.F. Silva, M. De Francesco, F. Cardellini, L. Giorgi, Electrochim. Acta 48 (3) (2002) 255.
[18] H.A. Gasteiger, P.N. Ross Jr., E.J. Cairns, Surf. Sci. 293 (1–2) (1993) 67.
[19] W.F. Lin, M.S. Zei, M. Eiswirth, G. Ertl, T. Iwasita, W. Vielstich, J. Phys. Chem. B 103 (33) (1999) 6968.
[20] B. Alvarez, A. Berna, A. Rodes, J.M. Feliu, Surf. Sci. 573 (1) (2004) 32.
[21] D.J. Watson, G.A. Attard, Surf. Sci. 515 (1) (2002) 87.
[22] J. Solla-Gullón, V. Montiel, A. Aldaz, J. Clavilier, Electrochem. Commun. 4 (9) (2002) 716.
[23] D.J. Watson, G.A. Attard, Electrochim. Acta 46 (20–21) (2001) 3157.
[24] R. Gómez, A. Rodes, J.M. Perez, J.M. Feliu, A. Aldaz, Surf. Sci. 344 (1–2) (1995) 85.
[25] G.A. Attard, A. Bannister, J. Electroanal. Chem. 300 (1–2) (1991) 467.
[26] J.L. Rousset, F.J. Cadete Santos, Appl. Surf. Sci. 164 (1–4) (2000) 163.
[27] J.L. Rousset, B.C. Khanra, A.M. Cadrot, F.J.C.S. Aires, A.J. Renouprez, M. Pellarin, Surf. Sci. 352–354 (1996) 583.
[28] J.A. Rodriguez, C.M. Truong, D.W. Goodman, Surf. Sci. 271 (1–2) (1992) L331.
[29] T. Itoyama, M. Wilde, M. Matsumoto, T. Okano, K. Fukutani, Surf. Sci. 493 (1–3) (2001) 84.
[30] R.T.S. Oliveira, M.C. Santos, L.O.S. Bulhoes, E.C. Pereira, J. Electroanal. Chem. 569 (2) (2004) 233.
[31] R.T.S. Oliveira, M.C. Santos, B.G. Marcussi, P.A.P. Nascente, L.O.S. Bulhoes, E.C. Pereira, J. Electroanal. Chem. 575 (2) (2005) 177.
[32] R. Gómez, F.J.G. de Dios, J.M. Feliu, Electrochim. Acta 49 (8) (2004) 1195.
[33] F.J.G. de Dios, R. Gómez, J.M. Feliu, Electrochem. Commun. 3 (11) (2001) 659.
[34] R. Gómez, J.M. Feliu, Electrochim. Acta 44 (6–7) (1998) 1191.
[35] J. Inukai, M. Ito, J. Electroanal. Chem. 358 (1993) 307.
[36] J. Datta, S.S. Gupta, J. Electroanal. Chem. 594 (1) (2006) 65.
[37] F.H.B. Lima, D. Profeti, W.H. Lizcano-Valbuena, E.A. Ticianelli, E.R. Gonzalez, J. Electroanal. Chem. 617 (2) (2008) 121.
[38] A. Kowal, S.L. Gojkovic, K.S. Lee, P. Olszewski, Y.E. Sung, Electrochem. Commun. 11 (4) (2009) 724.
[39] G.A. Attard, K.G. Griffin, D.J. Jenkins, P. Johnston, P.B. Wells, Catal. Today 114 (4) (2006) 346.
[40] R. Gómez, A. Rodes, J.M. Perez, J.M. Feliu, A. Aldaz, Surf. Sci. 327 (3) (1995) 202.
[41] M. Arenz, V. Stamenkovic, P.N. Ross, N.M. Markovic, Surf. Sci. 573 (1) (2004) 57.
[42] M. Arenz, V. Stamenkovic, T.J. Schmidt, K. Wandelt, P.N. Ross, N.M. Markovic, Phys. Chem. Chem. Phys. 5 (19) (2003) 4242.
[43] R.W. Evans, G.A. Attard, J. Electroanal. Chem. 345 (1–2) (1993) 337.
[44] F.J.G. de Dios, R. Gómez, J.M. Feliu, Langmuir 21 (16) (2005) 7439.
[45] M. Taniguchi, E.K. Kuzembaev, K.-i. Tanaka, Surf. Sci. Lett. 290 (3) (1993) L711.
[46] http://www.nist.gov/srd/nist100.cfm.
[47] M.T.M. Koper, S.C.S. Lai, E. Herrero, Mechanisms of the Oxidation of Carbon Monoxide and Small Organic Molecules at Metal Electrodes, in: M.T.M. Koper, Fuel Cell Catalysis, A Surface Science Approach, John Wiley & Sons, Inc., Hoboken, NJ, 2009, p. 159.
[48] P. Jeong Young, Z. Yawen, M. Grass, Z. Tianfu, G.A. Somorjai, Nano Lett. 8 (2) (2008) 673.
[49] C. Wang, M. Chi, D. Li, D. Strmcnik, D. van der Vliet, G. Wang, V. Komanicky, K.-C. Chang, A.P. Paulikas, D. Tripkovic, J. Pearson, K.L. More, N.M. Markovic, V.R. Stamenkovic, J. Am. Chem. Soc. 133 (36) (2011) 14396.